Extracting gravity wave parameters during the September 2002 Southern Hemisphere major sudden stratospheric warming using a SANAE imaging riometer

Nkanyiso Mbatha, Venkataraman Sivakumar, Hassan Bencherif, Sandile B. Malinga

Annales
Geophysicae
Open Access

Extracting gravity wave parameters during the September 2002 Southern Hemisphere major sudden stratospheric warming using a SANAE imaging riometer

N. Mbatha[1,2], V. Sivakumar[2], H. Bencherif[3], and S. Malinga[1]

[1]South African National Space Agency, Space Science, P.O. Box 32, Hermanus 7200, South Africa
[2]School of Chemistry and Physics, University of KwaZulu-Natal, Durban 4000, South Africa
[3]Laboratoire de l'Atmosphère et des Cyclones, UMR 8105 CNRS, Université de La Réunion, 97715 Saint-Denis, Cedex 9, La Réunion, France

Correspondence to: N. Mbatha (nmbatha@sansa.org.za)

Abstract. Using absorption data measured by imaging riometer for ionospheric studies (IRIS) located at the South Africa National Antarctic Expedition (SANAE), Antarctica (72° S, 3° W), we extracted the parameters of gravity waves (GW) of periods between 40 and 50 min during late winter/spring of the year 2002, a period of the unprecedented major sudden stratospheric warming (SSW) in the Southern Hemisphere middle atmosphere. During this period, an unprecedented substantial increase of temperature by about 25–30 K throughout the stratosphere was observed. During the period of the occurrence of the major stratospheric warming, there was a reduction of both the GW horizontal phase speeds and the horizontal wavelengths at 90 km. The GW phase speeds and horizontal wavelengths were observed to reach minimum values of about $7 \, \mathrm{m \, s^{-1}}$ and 19 km, respectively, while during the quiet period the average value of the phase speed and horizontal wavelength was approximately $23 \, \mathrm{m \, s^{-1}}$ and 62 km, respectively. The observed event is discussed in terms of momentum flux and also a potential interaction of gravity waves, planetary waves and mean circulation.

Keywords. Meteorology and atmospheric dynamics (middle atmosphere dynamics)

1 Introduction

The sudden stratospheric warming (SSW) is a dramatic thermo-dynamical event which involves considerable changes of the background wind, temperature and circulation of the winter high-latitude middle atmosphere (20–100 km). The primary mechanism behind the SSW relates to the growth of the upward-propagating transient planetary waves of wavenumber $s = 1$ or $s = 2$ and their nonlinear interaction with the zonal-mean flow in the stratosphere (Matsuno, 1971). This interaction decelerates and/or even reverses the eastward zonal wind in the winter stratosphere–mesosphere system. Moreover, this dramatic phenomena induces a downward circulation in the stratosphere, causing adiabatic heating and upward circulation in the mesosphere, resulting in adiabatic cooling (Liu and Roble, 2002; Coy et al., 2005; Mbatha et al., 2010).

The deceleration and reversal of the eastward polar night jet in the high-latitude stratosphere also changes the filtering of internal gravity waves (GW) and allows for increasing amounts of eastward-propagating GWs from the troposphere to penetrate into the mesosphere–lower thermosphere (MLT) and break there, while blocking westward-propagating GWs (Sathishkumar and Sridharan, 2009). These GWs are mesoscale phenomena that have important global effects on the circulation, temperature structure, chemistry and composition of the entire atmosphere (Alexander and Dunkerton, 1999). During the SSW, stationary GWs are absorbed by the mean atmosphere as they approach the zero mean zonal wind level. The interaction of GWs and winds during the stratospheric warming has significant impacts on the structure and general circulation in the mesosphere.

There have been several observational studies to examine GWs during the SSW period in the past decades. Using temperature profiles measured by Challenging Mini-satellite Payload (CHAMP) global positioning system (GPS) occultations, Ratnam et al. (2004) analysed the GW activity during the 2002 late winter/spring SSW in the Southern Hemisphere (SH). In their study, they showed that during the SSW period the GW energy (potential energy E_p) became three times higher than usual. Wang and Alexander (2009) used temperature retrievals from the Constellation Observation System for Meteorology, Ionosphere, and Climate (COSMIC)/Formosa Satellite Mission 3 (FORMOSAT-3), CHAMP/GPS radio occultation profiles and independent temperature retrievals from the EOS satellite High Resolution Dynamics Limb Sounder (HIRDLS) and Sounding of the Atmosphere using Broadband Emission Radiometry (SABER) aboard the Thermosphere Ionosphere Mesosphere Energetics & Dynamics (TIMED) satellite to investigate the SSW event and accompanying GW temperature amplitude in the 2007–2008 Northern Hemisphere (NH) winter. They reported enhancement of GW amplitudes in the stratosphere and subdued GW amplitudes in the mesosphere. Recently, a study by Yamashita et al. (2010) showed that the GW forcing controls the pattern and strength of residual circulation and thereby the characteristics of cooling and warming regions. They also showed that the planetary wave forcing in the MLT affects the vertical depth and magnitude of the MLT temperature anomalies through further modifying the residual circulation.

GWs are usually studied using radars, lidars and airglow imagers. In this study, a technique to extract GW parameters from imaging riometer absorption data first described by Jarvis et al. (2003) was used. Jarvis et al. (2003) used this technique for the first time, and performed observations of GWs using an imaging riometer located at Halley, Antarctica (76° S, 27° W). The technique uses fluctuations from ionospheric absorption as a tracer for GWs. Imaging riometers respond to changes in the absorption of the cosmic radio noise in the ionospheric D region, which enables them to detect the compression and rarefaction at ∼ 90 km altitude generated by the passage of GWs (Jarvis et al., 2003). In this work, Jarvis et al. (2003) demonstrated that a single wave absorbed in a co-located airglow imager was also present in the central beams of the Halley imaging riometer. The wave first appeared in the airglow imager at 07:25 UTC on the 7 June 2000, while it was not apparent in the imaging riometer data until 08:00 UTC. The work by Jarvis et al. (2003) was further extended by Moffat-Griffin et al. (2008), who also showed the capabilities of the imaging riometer to detect short-period mesospheric GWs using the fluctuation of the ionospheric absorption of cosmic radio noise. Moffat-Griffin et al. (2008) presented a detailed analysis technique for quantifying these signatures. They demonstrated the extraction of the wave period, horizontal phase speeds and horizontal wavelengths by applying wavelet analysis to synthetic imaging riometer absorption data. They also performed comparisons between the GW parameters extracted from imaging riometer data with those derived from a co-located airglow imager, and found good agreement between the two instruments. There have been no studies of short-period GWs using the South Africa National Antarctic Expedition (SANAE, 72° S, 3° W) imaging riometer before. Some of the studies which employed this instrument include the observation of energetic electron precipitation at SANAE IV, Antarctica, by Wilson and Stoker (2002), and spatial structures in enhanced ionization of the ionosphere observed by absorption of cosmic radio waves by Wilson et al. (2001).

In this study, the UK Meteorological Office (UKMO) assimilation temperature and zonal wind data are used to identify the SH 2002 late winter/spring major SSW as well as to examine variations of temperature and zonal wind in the stratosphere during the major SSW event. The SANAE SuperDARN HF radar wind data are to investigate the mean wind in the mesosphere–lower thermosphere (MLT) region. In the present work, the above-mentioned technique is used to extract parameters of GWs of periods between 40 and 50 min during the 2002 major SSW event (from 11 September (day 254) to 11 October (day 284) 2002) in the Southern Hemisphere over SANAE. We also compare the 2002 (SSW year) results with the results of 2003 (a year without a stratospheric warming). The SANAE imaging riometer is used for the first time to study mesospheric GWs signatures, and it will be for the first time that any imaging riometer is used to study GWs during the SSW.

2 Instruments and data

2.1 SANAE HF radar

The SANAE HF radar is part of the SuperDARN radar network, and it is located in Antarctica (72° S, 3° W). SuperDARN (Greenwald et al., 1995) is a network of HF radars originally designed to study plasma flow in the high-latitude ionosphere. A study by Hall et al. (1997) confirmed that echoes at ranges close to the SuperDARN radars are actually due to scatter from meteor trails near approximately 94 km altitude, except during periods of high K_p (an indication of geomagnetic disturbance). Hence, the near-range scatter can be utilized to study neutral winds at meteor heights. The SuperDARN radar network consists of a total of about 17 radars in the Northern Hemisphere and 9 in the Southern Hemisphere. The SuperDARN radars operate at frequencies between 8 and 20 MHz. Each radar site consist of a 16-antenna array connected to a phasing matrix which permits the single beam to be swept through 16 successive positions in increments of 3.25°, covering a sector with a nominal azimuth of 52°. The azimuthal resolution depends on the operating frequency and it ranges from 2.5° at 20 MHz to 6° at 8 MHz. The peak power is about 10 kW and the range resolution is 30–45 km with a typical pulse width of 200–300 μs.

Measurements are taken every 7 s at each of the 16 beam positions. The backscatter information from these pulses is sampled and then processed, giving multi-lag autocorrelation functions (ACFs). The ACFs are thereafter used to deduce backscatter power, mean Doppler velocity and the width of the Doppler power spectrum for each range with significant returns. The pulse sequence is about 40 ms in duration, and they are separated by 60 ms, resulting in 60 ACFs in each of the 7 transmitting seconds, which are averaged for each measurement. The measurements can be taken for up to 75 range gates along the beam, where each range gate is equal to 45 km. Thus, this means that the measurements can be made from a few kilometres to more than 3000 km in range.

The meteor trail echoes occur predominantly in and below the lower E region ($\sim$ 95 km) (Hussey et al., 2000); thus acquisition of the winds in the meteor region is accomplished by using data from the first several range gates of the radar. The backscatter at this distance is primarily due to meteors, and thus a nominal height of 90–95 km is assumed. Hourly wind averages are computed for each beam direction, giving a line-of-sight wind velocity. In the present work, these hourly wind averages are used to study the momentum flux in the MLT. More details about SuperDARN radars are given in a study by Greenwald et al. (1995).

2.2 The imaging riometer at SANAE

The imaging riometer at SANAE is a 64-element imaging riometer based on the design by Detrick and Rosenberg (1990). The instrument was constructed by the Department of Electronic Services, Potchefstroom University, South Africa, with continuous operation starting on 10 April 1997. This design of imaging riometer is an advance on the basic riometer as it utilizes narrow-beam antenna arrays to spatially sample the region of interest in contrast with a specially isolated measurement from a single wide beam.

Basically, riometers measures the intensity of the cosmic radio noise received at the surface of the Earth. As radio noise propagates through the atmosphere to the Earth's surface it suffers absorption because the radio waves excite the ionized plasma of the ionosphere, which then loses energy by electron and neutral air collision. Riometer frequencies are usually between 28 and 40 MHz, and these frequencies results in a maximum peak of absorption around the 90 km altitude in the D region of the atmosphere (Friedrich and Torkar, 1983). If there is absorption in the atmosphere, then the intensity of the cosmic radio noise received at the surface of the Earth decreases, and hence the absorption can be determined. However, if no absorption occurs, then the intensity of the cosmic radio signal received at the surface of the Earth is cyclic, with the period of a sidereal day; this signal is known as a quiet day curve. Riometers are primarily used to measure enhancement of the D-region ionosphere by energetic charged particle precipitation driven by magnetospheric electrodynamics (Stauning, 1984).
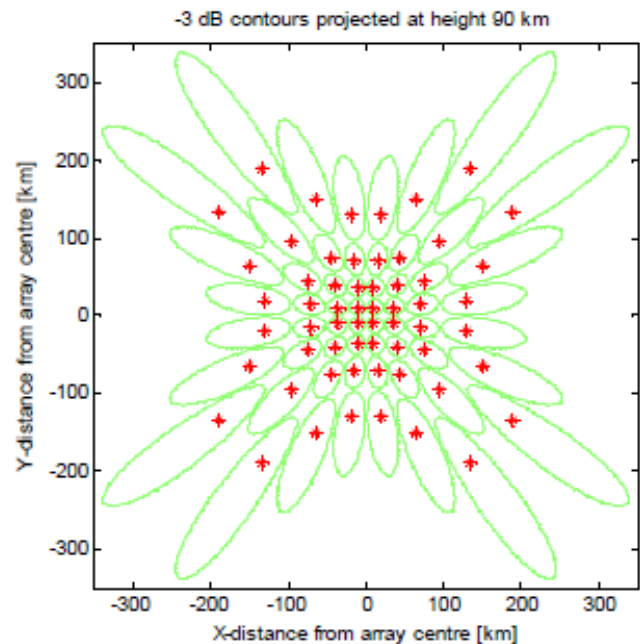

Fig. 1. Projection of the 3 dB contour of the 64-element imaging riometer beams onto a horizontal plane at 90 km altitude.

The imaging riometer for ionospheric studies (IRIS) at SANAE has 8×8 antenna arrays and consists of 64 half-wavelength crossed-dipole (turnstile) antennas mounted one quarter of a wavelength above an artificial ground plane (Wilson et al., 2001). Similar to the imaging riometer at Halley, the riometer at SANAE operates on 38.2 MHz and samples a region of over $200\,km \times 200\,km$ at 90 km altitude with 49 means every second (Detrick and Rosenberg, 1990). The details of the imaging riometer at SANAE are well explained by Wilson (2000). The projection of the riometer beams at 90 km altitude as defined by 3 dB beam projections is shown in Fig. 1. The separation between the circular beams projections near the centre is about 22 km, and the separation between the non-central elliptical beam projections in significantly larger.

As GWs have periods which are not discrete, it is necessary to determine first the dominant spectral components within the frequency band of interest. For this purpose, Fourier transform of the time series was performed. This analysis technique is an established tool for addressing localized variations of power within a time series. The details about Fourier transforms are well explained by Priestley (1981) and by Torrence and Compo (1998).

A study by Moffat-Griffin et al. (2008) used the wavelet squared coherence technique (Torrence and Webster, 1999), which effectively measures the cross-correlation between two wavelets' power spectra, to identify potential wave features that occur at the same period and time range in two time series. In the present work, we use the Fourier cross-spectrum to determine the dominant spectral components in
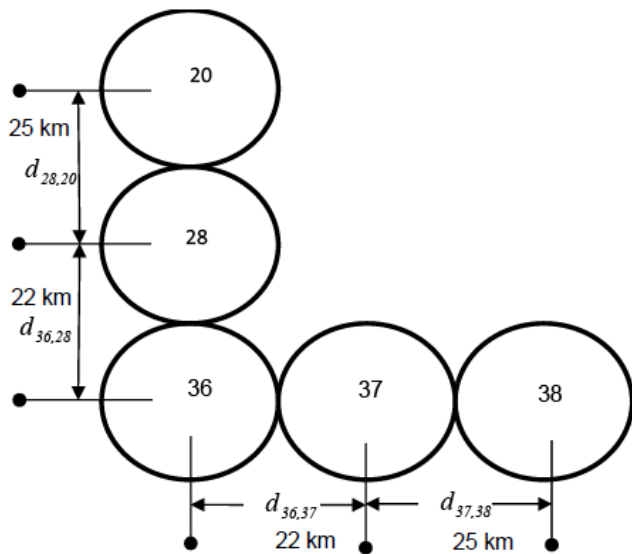
Fig. 2. The SANAE imaging riometer central beams and their beam separations.

two time series. The Fourier cross-spectra phase (Priestley, 1981), which is given by the average value of the phase shift between the two time series is the key parameter required for extraction of GW using imaging riometer. The projection of the riometer beams at 90 km altitude as defined by 3 dB beam peak projections is shown in Fig. 1. Similar to the work by Moffat-Griffin et al. (2008), we use the riometer centre beams 20, 28, 36 (northwards beams) and 36, 37, 38 (westwards beams), as labelled in Fig. 2.

The spatial resolution of the imaging riometer puts limitation on the resolvable horizontal wavelength in such a way that any wave that passes through the field of view with horizontal wavelengths shorter than the limit would be subjected to spatial aliasing, resulting in parameters obtained being unreliable (Moffat-Griffin et al., 2008). Thus, in the present work, we also adjust the phase difference ratio using $\pm 2n\pi$ (where n is any integer) until the best match to the beam separation if found.

2.3 UK Met Office data

The UKMO assimilation system (Swinbank and O'Neill, 1994) is an outcome of assimilation of in situ and remotely sensed data into a numerical forecast model of the stratosphere and troposphere. The outputs of the assimilation are global fields of daily temperature, geopotential height and wind components (meridional and zonal) at pressure levels from the surface up to 0.1 hPa. The assimilation system uses a global 42-level configuration of the unified mode with a horizontal resolution of 2.5° and 3.75° steps in latitude and longitude, respectively, and has been run daily since October 1991 to produce near-real-time global stratospheric analyses at ∼ 12:00 UTC every day. The analyses are output on

the Upper Atmosphere Research Satellite (UARS) standard levels from 1000 to 0.316 hPa. The description of the original data assimilation system can be found in the work published by Swinbank and O'Neill (1994); the updated version, which uses a three-dimensional variational data assimilation system, is found in the work by Lorenc et al. (2000) and also Swinbank and Ortland (2003).

3 Results and discussion

3.1 SH 2002 SSW event

Figure 3 shows the time–height contour plot of UKMO zonal-mean temperature at 80° S and latitude contour plot of zonal-mean zonal wind at 60° S for the period from 1 June 2002 to 31 October 2002. The SH polar stratosphere was relatively quiet until observation of minor warmings in late August and early September preceding major stratospheric warming in late September. The major stratospheric warming period is indicated by a black rectangle in Fig. 3. An unprecedented substantial increase of temperature by about 25–30 K throughout the stratosphere is observed in late September. On the day 269 (26 September 2002) the WMO (Andrews et al., 1987) criterion (which was also used for the widely known STRATALERT messages by Labitzke and Naujokat, 2000) of a major warming is fulfilled with the increase (by more than 25 K) of zonal-mean temperature at 80° S at 10 hPa pressure level and the reversal of zonal-mean zonal wind. During this event the polar vortex also split, causing the normally quiescent Antarctica ozone hole to also split into two parts (Baldwin et al., 2003; Bencherif et al., 2007). The details of the dynamics of the 2002 stratospheric warming has been reported by authors such as Baldwin et al. (2003), Dowdy et al. (2004), Ren et al. (2008), Mbatha et al. (2010) and Azeem et al. (2010).

3.2 GWs parameters

The times series showing imaging riometer absorption for the five SANAE imaging riometer centre beams labelled in Fig. 1 are shown in Fig. 4. These riometer absorption subfigures are for day number 259 (16 September 2002) of the year 2002, and they serve as an example of the SANAE imaging riometer absorption time series used in this study. All the selected riometer beams show similar behaviour of absorption during this day. In order to identify the dominant period in fluctuations of absorption, wavelet transforms were applied to the absorption time series. Figure 5 shows the diagrams of normalized wavelet power spectra of the five centre beams to show the periods of GWs available in the time series. In this figure, the solid black contour encloses regions of greater than 95 % confidence level for a red-noise process with a lag-1 coefficient (α) of 0.72 (e.g. Torrence and Compo, 1998). The red lines at both ends indicate the "cone of influence", where the edge effects become
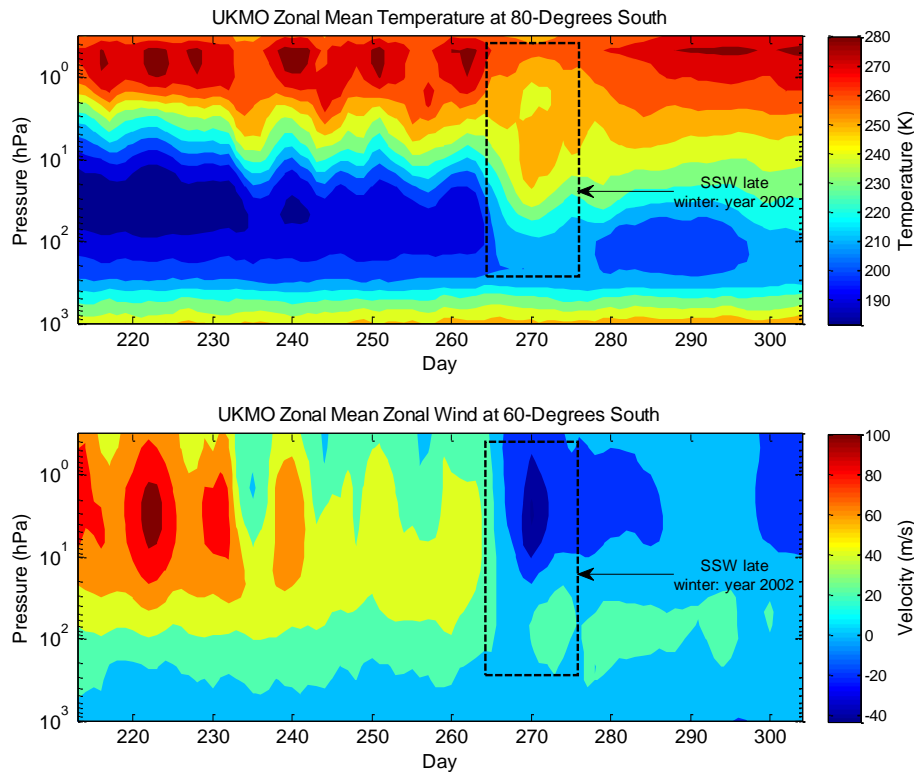
Fig. 3. (a) Daily zonal-mean temperature at 80° S for the period from 1 June to 31 October 2002. **(b)** Daily zonal-mean zonal wind at 60° S for the same period. The black box indicates the period of the occurrence of the year 2002 SSW.

important (Torrence and Compo, 1998). The same wavelet power spectra (not shown in this paper) are computed for days before, during and after the stratospheric warming for the purpose of extracting GW parameters during these periods. Because in the present work we intend to focus on short-period GWs, a band-pass fast Fourier transform (FFT) filter was used to filter periods less than 3 min and greater than 60 min. What is noticeable is that the spectra of the five riometer beams in Fig. 5 show significant GW of periods greater than 20 min. Figure 6 also shows the normalized wavelet power spectra for the centre beam number 36 for the day number 255 (12 September 2002), 267 (24 September 2002) and 274 (1 October 2002), respectively. These days were selected in order to show the GW activity before, during and after the SSW. From this figure, it is observed that in all the days there is a signature of GWs of period between 10 and 50 min. An interesting feature is that of a weaker power of gravity waves during the period of the occurrence of the SSW. The same feature was observed with the other days that are not shown in this paper. For the purpose of this study, only GW periods between 40 and 50 min are used because of their dominance after the filter limitations application.

For the purpose of calculating the horizontal phase speed and horizontal wavelength, the important parameter is the phase shift of the wave of interest as observed by the centre beam used in this study. Therefore, wavelet power spectra

in Fig. 5 are only used to identify the available GW periods of interest in the time series, and the phase shift was calculated using Fourier transform. The important criterion was to consider only those periods which had amplitudes above the 95 % confidence level using a chi-square test, assuming white noise as background spectrum (Torrence and Compo, 1998), in a normalized Fourier power spectra of the five centre beams. Also, only the days where the disturbance storm time (Dst) value averaged for a day was above −50 nT were considered, because this indicates low magnetic storm activity (Gonzalez et al., 1984). The Fourier cross-spectrum effectively measuring the cross-correlation between two Fourier power spectra is used to identify potential wave features that occur at the same period and time range in the two time series. The Fourier coherency phase difference between these coherent features was also calculated. This phase spectrum is expressed as

$$\varphi_{xy}(\omega) = \arctan\left(\frac{q_{xy}(\omega)}{c_{xy}(\omega)}\right), \tag{1}$$

where $c_{xy}(\omega)$ and $q_{xy}(\omega)$ are co-spectrum and quadrant spectrum representing the covariance between the coefficients of the in-phase and the quadrature components of the original signals $x(t)$ and $y(t)$, respectively (Chatfield, 1989). The above equation represents the average value of the phase shift $\{\varphi_x(\omega) - \varphi_y(\omega)\}$ between the components of the two
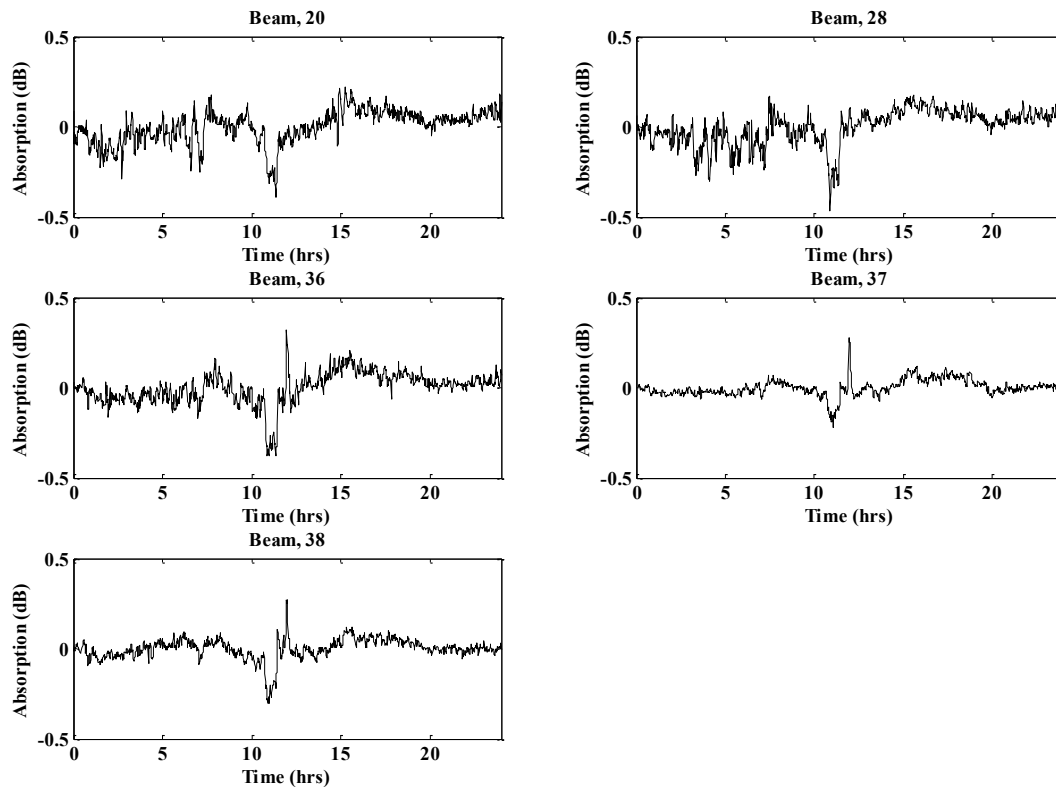
Fig. 4. Radio absorption measured by SANAE imaging riometer centre beams (20, 28, 36, 37 and 28) for day number 259 of the year 2002.

signals $x(t)$ and $y(t)$. The information about the distance between riometer centre beams at a given altitude is known (see Fig. 2), and also the period of the wave feature and its phase difference. With this information available, the horizontal phase speed and wavelength are calculated. The horizontal phase speed is determined by Eq. (2), and the horizontal wavelength is determined by Eq. (3):

$$V_{\mathrm{p}} = \frac{2\pi \Delta x}{\Delta \varphi T}, \qquad (2)$$

$$\lambda = \frac{2\pi \Delta x}{\Delta \varphi T}, \qquad (3)$$

where Δx is the distance between the beams, $\Delta \varphi$ is the phase difference between the beams in radians and T is the observer Doppler-shifted wave period in seconds. The special resolution of the imaging riometer puts limitations on the resolvable horizontal wavelength of $2\Delta x$, and this results in the lowest resolvable limit of 45 km for the horizontal wavelength of the centre beam (Moffat-Griffin et al., 2008). Thus, any wave that passes through the field of view with a horizontal wavelength shorter than this limitation will be subject to spatial aliasing resulting in unreliable calculation of parameters. In order to eliminate this complication, Moffat-Griffin et al. (2008) developed a method that requires a wave feature to be detected in three linearly adjacent beams over the

same period and time. More details about this method are explained by Moffat-Griffin et al. (2008).

When examining both the GW horizontal phase speeds and wavelengths, it is observed that the GWs of periods between 40 and 50 min can go up to a maximum of $29\,\mathrm{m\,s^{-1}}$ and 69 km on a normal period (without the major SSW). On average, the values of GW parameters calculated using SANAE imaging riometer is in agreement with observations by Moffat-Griffin et al. (2008), who used both the Halley imaging riometer and all-sky airglow imager and obtained GW horizontal phase speeds and wavelengths ranging from 9 to $56\,\mathrm{m\,s^{-1}}$ and from 14 to 60 km, respectively, on random days of the year 2000. However, an interesting observation in our results is that during the period of the major stratospheric warming (especially from day number 264 to 270), the GW horizontal phase speed and wavelength had the lowest values that could reach minimum values of approximately $7\,\mathrm{m\,s^{-1}}$ and 19 km, respectively. When comparing year 2002 to year 2003, it is clearly observed that both the phase speed and horizontal wavelength have comparable parameters for most of the days of the studied period, but the difference is observed during the period of the SSW event from day number 264 to 272. In Fig. 8a, SANAE HF radar zonal wind (ZW) at the MLT and National Centers for Environmental Prediction (NCEP) zonal-mean zonal wind at 10 hPa, respectively, was plotted against SANAE imaging
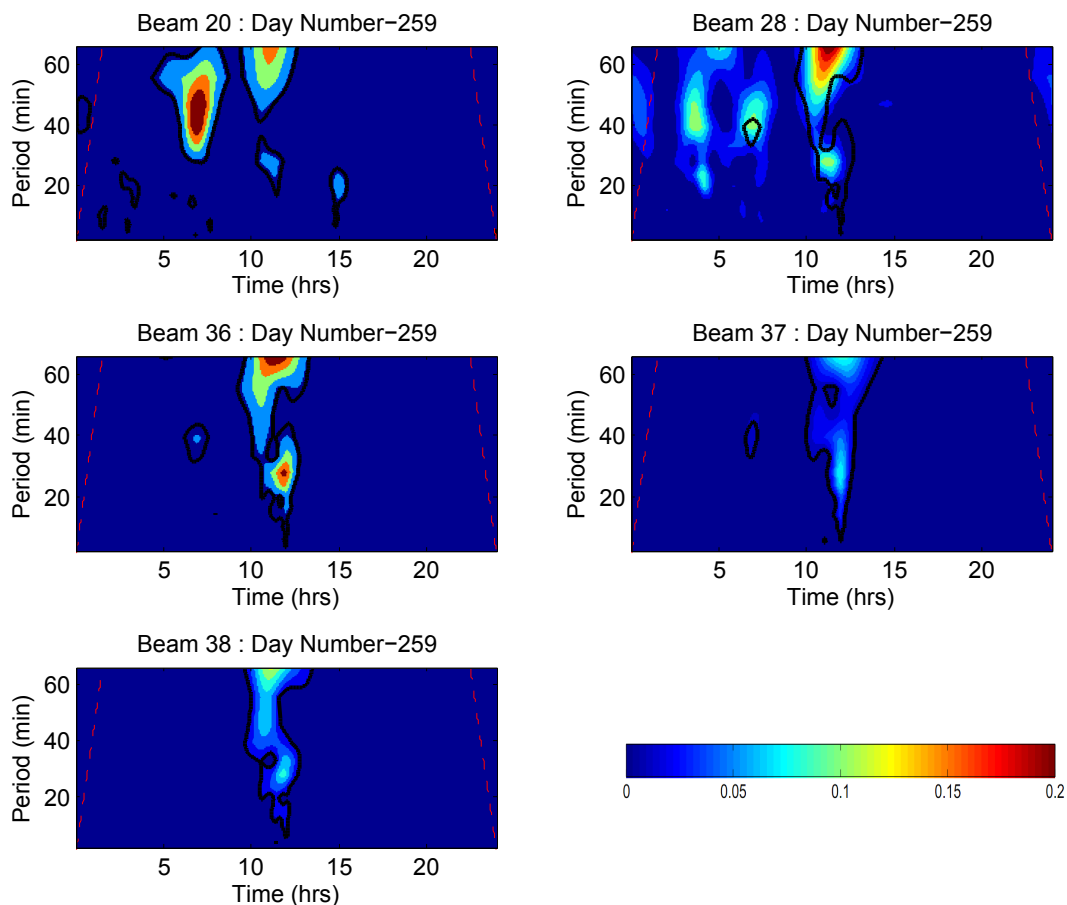
Fig. 5. Normalized wavelet power spectrum of radio absorption measured by SANAE imaging riometer centre beams (20, 28, 36, 37 and 28) for day number 259 of September 2002. The solid black contour encloses regions of greater than 95 % confidence level (red noise $\alpha = 0.72$). The red lines at both ends indicate the cone of influence.
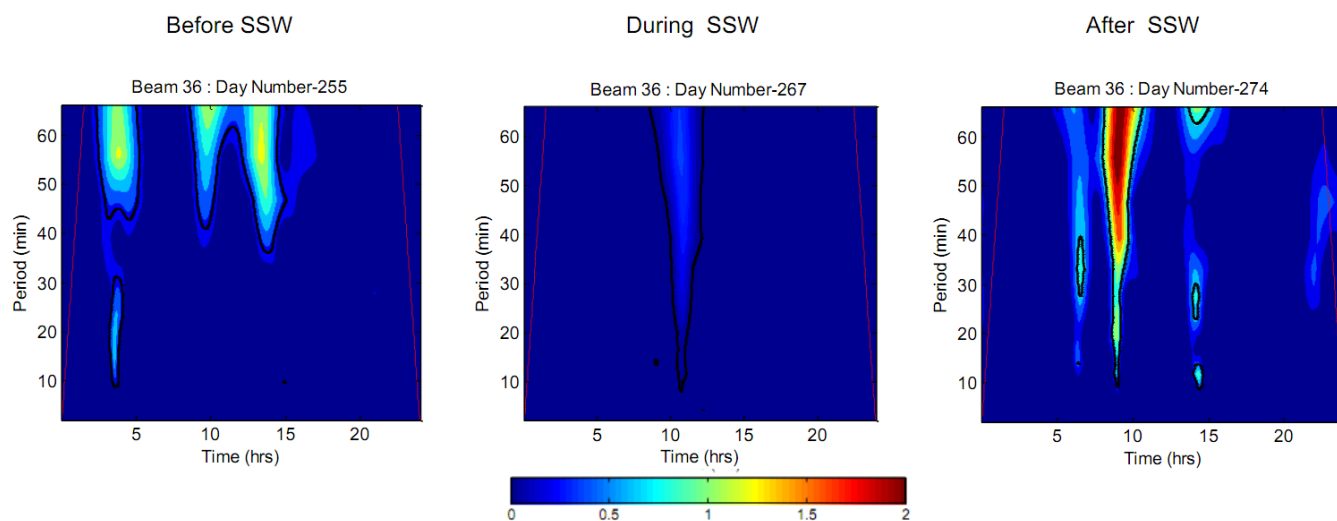

Fig. 6. Normalized wavelet power spectrum of radio absorption measured by SANAE imaging riometer centre beam number 36 for day 2 day which is two days before the SSW (left panel), during the SSW (centre panel) and after (right panel) the SSW. The solid black contour encloses regions of greater than 95 % confidence level (red noise $\alpha = 0.72$). The red lines at both ends indicate the cone of influence.
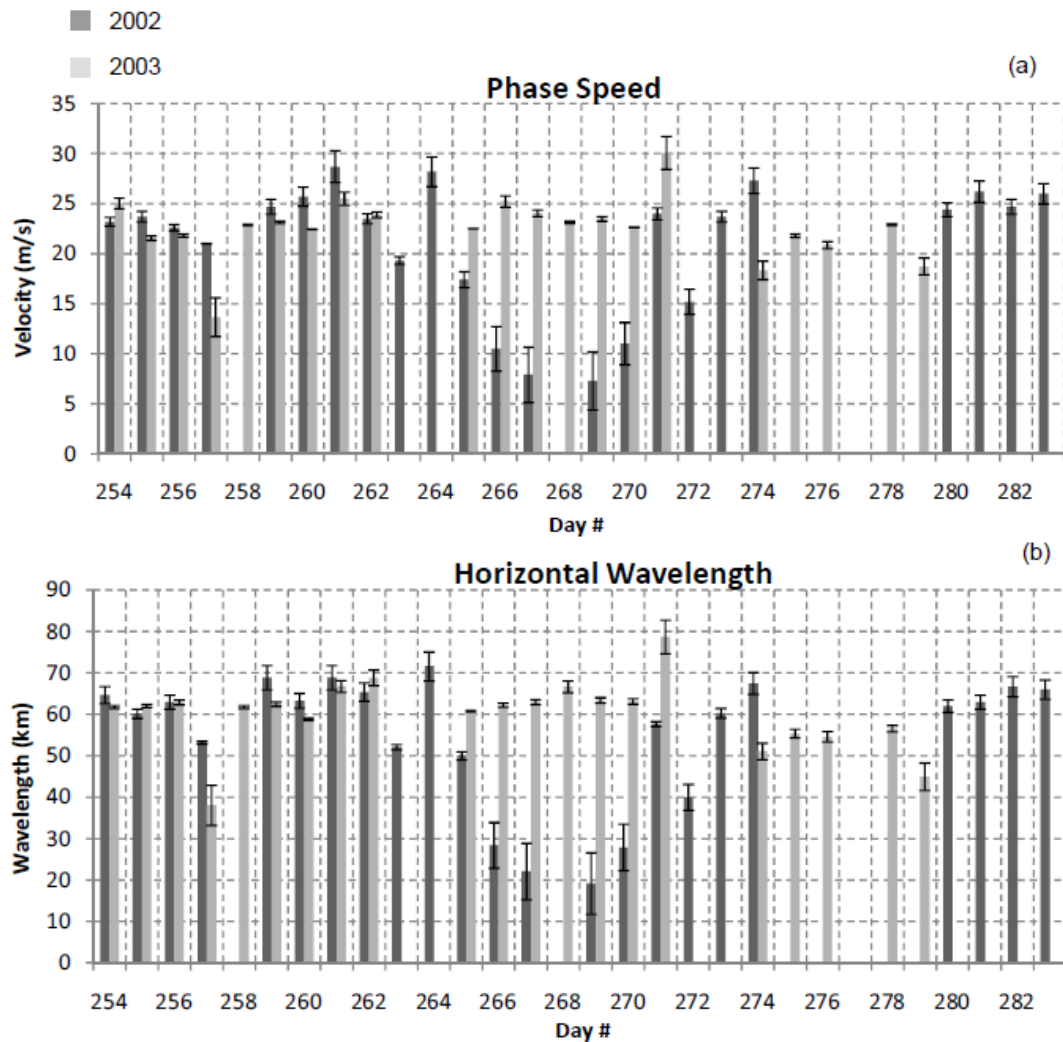
Fig. 7. Histograms showing GW phase speeds **(a)** and horizontal wavelengths **(b)** for the year 2002 (dark-grey bars) and 2003 (light-grey bars) day number from 254 to 282. The standard deviations are also included.

riometer GW phase speeds for the period of late winter of the year 2002. The SANAE HF zonal winds is made up of an hourly 4-day data window which was advanced by 1 day at a time, and the average of the data window was attributed to the second day of the interval. The 4-day mean was considered to be acceptable if at least 60 % of possible hourly wind values were recorded. Below it (Fig. 8b) is the plot for the imaging riometer horizontal wavelengths for the same period. Figure 8a is an improvement of the previous study by the author (Mbatha et al., 2010), where the zonal wind is indicated at 10 hPa, as derived from the NCEP during the period from day 250 to 300 in 2002 and superimposed the zonal wind observations from SANAE HF radar (for ±94 km MLT height). In their study, they showed that the zonal wind started to reverse (become westward) in the MLT region on day 261 of 2002 (18 September), i.e. about a week earlier than the reversal of the zonal wind in the polar stratosphere at

∼ 10 hPa pressure level. This behaviour indicates that there may be a downward propagation of circulation disturbance in the middle atmosphere. Similar results were also reported by Dowdy et al. (2004). In this study, the GW phase speeds calculated from SANAE imaging riometer are also plotted against the MLT and stratospheric zonal wind. The influence of the stratospheric warming in the GW phase speeds is apparent (see Fig. 8a). The same is observed in the GW horizontal wavelengths (see Fig. 8b). Both of these GW parameters are observed to commence their reduction in about three to four days before the reversal of the mean wind in the stratosphere, indicating the usually reported downward circulation disturbance in the atmosphere associated with the major stratospheric warming.

The low values of both the GW phase speeds and horizontal wavelengths during the occurrence period of the SSW as observed by the SANAE riometer may not be a surprise
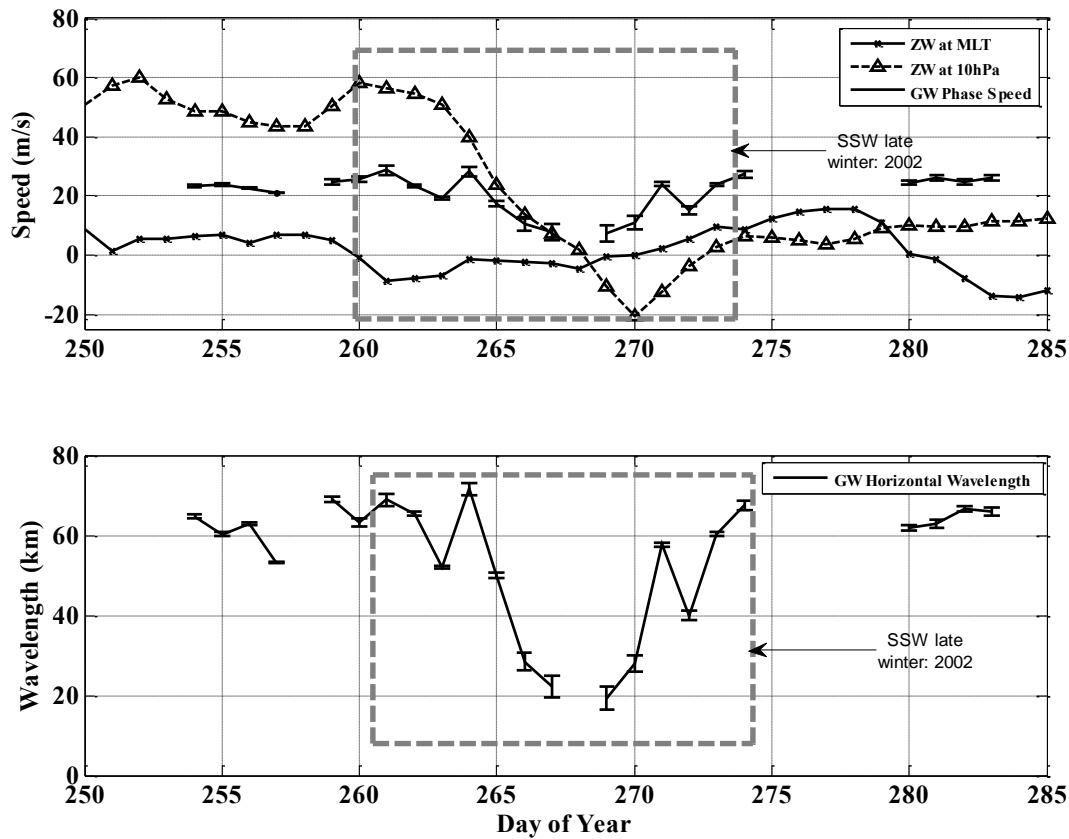
Fig. 8. (a) Time evolution of zonal wind (ZW) at the MLT (cross symbols) and at 10 hPa (triangle symbols), and GW phase speeds (square symbols) from 11 September to 11 August 2002. **(b)** Time evolution of GW horizontal wavelengths for the same period. The grey boxes indicate the period of the occurrence of the year 2002 SSW.

because the mesopause region may be the region where the wave breaking occurred, and thus the loss of the wave momentum. This wave breaking led to the cooling of the MLT and also the reversal of the mean circulation in the MLT in late September 2002 (Dowdy et al., 2004; Mbatha et al., 2010). This finding is consistent with the work published by Ratnam et al. (2004), who studied the enhancement of GW activity observed during the Southern Hemisphere stratospheric warming by Challenging Minisatellite Payload (CHAMP) global positioning system (GPS) measurements at high latitude region. In their study, they showed that the potential energy of GWs seems to decrease during the major SSW occurrence period in the height region between 25 and 30 km. This may be due to the interaction between GW and the dominant planetary waves of a period of 10–16 days which was observed in the stratosphere during the 2002 winter (Baldwin et al., 2003; Dowdy et al., 2004).

4 Summary and conclusions

In this study, the SANAE imaging riometer was used for the first time to extract GW parameters (phase speed and hori-

zontal wavelength). It was also the first time for the imaging riometer to be used to study the SSW event. We first identified the unprecedented year 2002 stratospheric warming by using the UKMO stratospheric wind and temperature fields. More details of the 2002 major stratospheric warming can be found in studies by Baldwin et al. (2003), Dowdy et al. (2004), Mbatha et al. (2010) and others. The mean circulation in the stratosphere was characterized by a series of planetary wave events in the 2002 winter that weakened the polar vortex and triggered the SSW in late September (Baldwin et al., 2003; Dowdy et al., 2004; Cho and Shepherd, 2004; Bencherif et al., 2007; Mbatha et al., 2010). A quasi-10-day wave of wavenumber $s = 1$ travelling in an eastward direction was identified as responsible for triggering the occurrence of the 2002 major SSW (Dowdy et al., 2004). Even the analysis of ozone from GOME showed that the ozone enhancement led to the smaller size of the Antarctica ozone hole in September 2002 (Baldwin et al., 2003; Allen et al., 2003). This was primarily due to the existence of higher temperatures than normal, and the disturbance in the mean circulation. This disturbance of the mean circulation and temperature was also detected in the MLT heights (Cho and Shepherd, 2004; Mbatha et al., 2010).

During the period of the occurrence of the major strato-spheric warming, there was a reduction of both the GW horizontal phase speeds and the horizontal wavelengths at 90 km. The GW phase speeds and horizontal wavelengths were observed to reach minimum values of about $7\,\mathrm{m\,s^{-1}}$ and 19 km, respectively, while during the quiet period the average value of the phase speed and horizontal wavelength was approximately $23\,\mathrm{m\,s^{-1}}$ and 62 km, respectively. This reduction of the above-mentioned parameters may be associated with the region where GWs break, and thus the loss of the wave momentum. This process also leads to mesospheric cooling (e.g. Cho and Shepherd, 2004; Mbatha et al., 2010; Yamashita et al., 2010). A study by Murphy et al. (2007) utilized MF radar wind measurements from Davis (68.35° S, 77.58° E) for the period from 1997 to 2005 to compile climatology of long-period wave activity in the MLT region. In this study, large positive momentum fluxes (figures are not shown) were observed prior to the occurrence of the year 2002 SSW. These momentum fluxes were associated with the amplification of the wave activity during the year 2002 winter in the Southern Hemisphere.

GWs are generated in the troposphere due to a variety of meteorological and orographic situations. These waves can have zonal asymmetry resulting from the distribution of orographic features and flows in the troposphere. But, in the Southern Hemisphere, these processes are limited due to the topographic situation, unlike in the Northern Hemisphere. GWs propagate up to the MLT altitude, but in some cases they are filtered by the stratosphere circulation, which may be zonally asymmetric due to planetary waves. At the MLT heights, the present study seems to indicate that the GWs dissipate and deposit their momentum in late winter 2002. The previous study by Mbatha et al. (2010) showed that during late winter 2002 there was presence of a quasi-14-day wave in the MLT, and this may indicate that when GWs dissipated in the MLT, the wave drag forcing may have a planetary-scale zonal asymmetry. While a study by Murphy et al. (2007) performed the climatology of the heat and momentum flux using wind and temperature data measured using the Davis MF radar and hydroxyl temperature, it would be interesting to use the SANAE SuperDARN HF radar wind data and satellite data to perform the heat and momentum flux climatology. Moreover, the analysis technique used in this study will be applied to the entire SANAE imaging riometer data set to build up the climatology of mesospheric GW characteristics over this region. The observations from the SANAE riometer will also be compared to other imaging riometers situated across Antarctica, as well as other instruments (e.g. airglow imager). This technique will also be used to study longer period (> 60 min) gravity waves as well in future.

References

Alexander, M. J. and Dunkerton, T. J.: A spectral parameterization of mean-flow forcing due to breaking GWs, J. Atmos. Sci., 56, 4167–4182, 1999.

Allen, D. R., Bevilacqua, R. M., Nedoluha, G. E., Randall, C. E., and Manney, G. L.: Unusual stratospheric transport and mixing during the 2002 Antarctic winter, Geophys. Res. Lett., 30, 1599, doi:10.1029/2003GL017117, 2003.

Andrews, D. G., Halton, J. R., and Leovy, C. B.: Middle Atmospheric Dynamics, 489 pp., Elsevier, New York, 1987.

Azeem, S. M. I., Talaat, E. R., Sivjee, G. G., and Yee, J.-H.: Mesosphere and lower thermosphere temperature anomalies during the 2002 Antarctic stratospheric warming event, Ann. Geophys., 28, 267–276, doi:10.5194/angeo-28-267-2010, 2010.

Baldwin, M., Hirooka, T., O'Neill, A., and Yoden, S.: Major stratospheric warming in the Southern Hemisphere in 2002: Dynamical aspect of the ozone hole split, SPARC Newsl, 20, 24–26, 2003.

Bencherif, H., Charyulu, D. V., Amraoui, L. E., Peuch, V.-H., Semane, N, and Hauchecorne, A.: Examination of the 2002 major warming in the southern hemisphere using ground-based and Odin/SMR assimilated data: stratospheric ozone distribution and tropic/mid-latitude exchange, Can. J. Phys., 85, 1287–1300, doi:10.1139/P07-143, 2007.

Chatfield, C.: The analyses of time series. An Introduction, Chapman & hall, London, 1989.

Cho, Y.-M. and Shepherd, G. G.: MLT cooling during stratospheric warming events, Geophys. Res. Lett., 31, L10104, doi:10.1029/2004GL019552, 2004.

Coy, L., Siskind, D. E., Eckermann, S. D., McCormack, J. P., Allen, D. R., and Hogan, T. F.: Modeling the August 2002 minor warming event, Geophys. Res. Lett., 32, L07808, doi:10.1029/2005GL022400, 2005.

Detrick, D. L. and Rosenberg, T. J.: A phased-array radiowave imager for studies of cosmic noise absorption, Radio. Sci., 25, 325–338, 1990.

Dowdy, A. J., Vincent, R. A., Murphy, D. J., Tsutsumi, M., Riggin, D. M., and Jarvis, M. J.: The large-scale dynamics of the Mesosphere-lower thermosphere during the Southern Hemisphere stratospheric warming of 2002, Geophys. Res. Lett., 31, L14102, doi:10.1029/2004GL020282, 2004.

Friedrich, M. and Torkar, K. M.: High-latitude plasma densities and their relation to riometer absorption, J. Atmos. Terr. Phys., 45, 127–135, 1983.

Gonzalez, W. D., Joselyn, J. A., Kamide, Y., Kroehl, H. W., Rostoker, G., Tsurutani, B. T, and Vasyliunas, V. M.: What is a geomagnetic storm?, J. Geophys. Res.: Space Physics, 99, 5771–5792, 1984.

Greenwald, R. A., Baker, K. B., Dudeney, J. R., Pinnock, M., Jones, T. B., Thomas, E. C., Villain, J.-P., Cerisier, J.-C., Senior, C.,

Hanuise, C., Hunsucker, R. D., Sofko, G., Koehler, J., Nielsen, E., Pellinen, R., Walker, A. D., Sato, N., and Yamagishi, H.: DARN/SuperDARN: A global view of the dynamics of high latitude convections, Space Sci. Rev., 71, 761–796, 1995.

Hall, G. E., MacDougall, J. W., Moorcroft, D. R, and St.-Maurice, J.-P.: Super Dual Auroral Radar Network observations of meteor echoes, J. Geophys. Res., 102, 14603–14614, 1997.

Hussey, G. C., Meek, C. E., André, A. H., Manson, A. H., Sofko, G. J., and Hall, C. M.: A comparison of Northern Hemisphere wind using SuperDARN meteor trail and MF radar wind measurements, J. Geophys. Res., 105, 18053–18066, 2000.

Jarvis, M. J., Hibbins, R. E., Taylor, M. J., and Rosenberg, T. J.: Utilizing riometry to observe GWs in the sunlit mesosphere, Geophys. Res. Lett., 30, 1979, doi:10.1029/2003GL017885, 2003.

Labitzke, K. and Naujokat, B.: The lower Arctic stratosphere in winter since 1952, SPARC Newsletter, 15, 11–14, 2000.

Liu, H.-L. and Roble, R. G.: A study of self-generated stratospheric sudden warming and it mesosphere-lower thermosphere impacts using the coupled TIME-GCM/CCM3, J. Geophys. Res., 107, 4695, doi:10.1029/2001JD001533, 2002.

Lorenc, A. C., Ballard, S. P., Bell, R. S., Ingleby, N. B., Andrews, P. L. F., Barker, D. M., Bray, J. R., Clayton, A. M., Dalby, T., Li, D., Payne, T. J., and Saunders, F. W.: The Meteorol. Office global 3-dimensional variational data assimilation scheme, Q. J. Roy. Meteorol. Soc., 126, 2991–3012, 2000.

Matsuno, T.: A dynamic model of the stratospheric sudden warming, J. Atmos. Sci., 28, 1479–1494, 1971.

Mbatha, N., Sivakumar, V., Malinga, S. B., Bencherif, H., and Pillay, S. R.: Study on the impact of sudden stratosphere warming in the upper mesosphere–lower thermosphere regions using satellite and HF radar measurements, Atmos. Chem. Phys., 10, 3397–3404, doi:10.5194/acp-10-3397-2010, 2010.

Moffat-Griffin, T., Hibbins, R. E., Nielsen, K., Jarvis, M. J., and Taylor, M. J.: Observing mesospheric GWs with an imaging riometer, J. Atmos. Sol. Terr. Phys., 70, 1327–1335, 2008.

Murphy, D. J., French, W. J. R., and Vincent, R. A.: Long-period planetary waves in the mesosphere and lower thermosphere above Davis, Antarctica, J. Atmos. Terr. Phys., 69, 2118–2138, 2007.

Priestley, M. B.: Spectral analysis and time series. Volume 2: Multivariate series, prediction and control, Academic Press, 1981.

Ratnam, M. V., Tsuda, T., Jacobi, C., and Aoyama, Y.: Enhancement of GW activity observed during a major Southern Hemisphere stratospheric warming by CHAMP/GPS measurements, Geophys. Res. Lett., 31, L16101, doi:10.1029/2004GL019789, 2004.

Ren, S., Polavarapu, S. M., and Shepherd, T. G.: Vertical propagation of information in a middle atmosphere data assimilation system by gravity-wave drag feedbacks, Geophys. Res. Lett., 35, L06804, doi:10.1029/2007GL032699, 2008.

Sathishkumar, S. and Sridharan, S.: Planetary and GWs in the mesosphere and lower thermosphere region over Tirunelveli (8.7° N, 77° E) during stratospheric warming events, Geophys. Res. Lett., 36, L07806, doi:10.1029/2008GL037081, 2009.

Stauning, P.: Absorption of cosmic noise in the E-region during electron heating events. A new class of riometer absorption events, Geophys. Res. Lett., 11, 1184–1187, 1984.

Swinbank, R. and O'Neill, A.: A Stratosphere-Troposphere Data Assimilation System, Mon. Weather Rev., 122, 686–702, 1994.

Swinbank, R. and Ortland, D. A.: Compilation of wind data for the Upper Atmosphere Research Satellite (UARS) Reference Atmosphere Project, J. Geophys. Res., 108, 4615, doi:10.1029/2002JD003135, 2003.

Torrence, C. and Compo, G. P.: A practical guide to wavelet analysis, B. Am. Meteorol. Soc, 79, 61–78, 1998.

Torrence, C. and Webster, P. J.: Interdecadal changes in the ENSO–monsoon system, J. Climate, 12, 2679–2690, 1999.

Wang, L. and Alexander, M. J.: GW activity during stratospheric sudden warmings in the 2007–2008 Northern Hemisphere winter, J. Geophys. Res., 114, D18108, doi:10.1029/2009JD011867, 2009.

Wilson, A.: Imaging riometer observations on energetic electron precipitation at SANAE IV, Antarctica, PhD thesis, Potchefstroomse Universiteit vir Christelike Hoër Onderwys, 2000.

Wilson, A. and Stoker, P. H.: Imaging riometer observations on energetic electron precipitation at SANAE IV, Antarctica, J. Geophys. Res., 107, 1268, doi:10.1029/2000JA000463, 2002.

Wilson, A., Nel, J. J., Mathews, M. J., and Stoker, P. H.: Direct measurements on imaging riometer antenna array beam directivities, Radio Sci., 36, 1531–1543, 2001.

Yamashita, C., Liu, H. L., and Chu, X.: Responses of mesosphere and lower thermosphere temperatures to GW forcing during stratospheric sudden warming, Geophys. Res. Lett., 37, L09803, doi:10.1029/2009GL042351, 2010.